

Article

MoS₂ Quantum Dot Modified Electrode: An Efficient Probe for Electrochemical Detection of Hydrazine

Susmita Roy ¹, Sarda Sharma ², Karumbaiah N. Chappanda ^{2,3}  and Chanchal Chakraborty ^{1,3,*} 

¹ Department of Chemistry, Birla Institute of Technology and Sciences (BITS), Pilani, Hyderabad Campus, Hyderabad 500078, Telangana, India

² Department of Electrical and Electronics Engineering, Birla Institute of Technology and Sciences (BITS), Pilani, Hyderabad Campus, Hyderabad 500078, Telangana, India

³ Materials Center for Sustainable Energy & Environment (McSEE), Birla Institute of Technology and Sciences (BITS), Pilani, Hyderabad Campus, Hyderabad 500078, Telangana, India

* Correspondence: chanchal@hyderabad.bits-pilani.ac.in

Abstract: The development of an effective sensor system that can detect carcinogenic hydrazine is of prime scientific interest for the protection of human health and the environment. In the present study, MoS₂ quantum dots (QDs) with an average diameter of ~5 nm were synthesized using a facile one-step, bottom-up hydrothermal method using cysteine as reducing as well as capping agents. The presence of cysteine was evaluated by FTIR spectroscopy. The synthesized MoS₂ QDs were applied to modify the conventional glassy carbon electrode (GCE) in order to detect hydrazine electrochemically in neutral pH conditions. In the cyclic voltammetry (CV) study, the MoS₂ QDs-modified electrode revealed much better catalytic activities for hydrazine electro-oxidation compared to the bare GCE surface. The smaller size of the QDs with high surface area and the presence of carboxylic acid containing cysteine on the surface of the QDs enhanced the adsorption as well as the electrocatalytic activity. The amperometric response of MoS₂-QD-modified GCE unveiled excellent electrocatalytic sensing properties towards neurotoxic hydrazine with a very high sensitivity of 990 μAmM⁻¹cm⁻² (R² = 0.998), low LOD of 34.8 μM, and a broad linear range. Moreover, this high-sensitive, binder and conducting filler-free MoS₂-QD-based sensing system is very promising in agile amperometric detection of neurotoxic hydrazine for environmental monitoring in industrial sectors.

Keywords: MoS₂ QDs; hydrazine; electrochemical sensing; electro-oxidation; modified electrode



Citation: Roy, S.; Sharma, S.; Chappanda, K.N.; Chakraborty, C. MoS₂ Quantum Dot Modified Electrode: An Efficient Probe for Electrochemical Detection of Hydrazine. *Designs* **2023**, *7*, 13. <https://doi.org/10.3390/designs7010013>

Academic Editor: Richard Drevet

Received: 10 December 2022

Revised: 31 December 2022

Accepted: 6 January 2023

Published: 12 January 2023



Copyright: © 2023 by the authors. Licensee MDPI, Basel, Switzerland. This article is an open access article distributed under the terms and conditions of the Creative Commons Attribution (CC BY) license (<https://creativecommons.org/licenses/by/4.0/>).

1. Introduction

Hydrazine and its derivatives are the low molecular weight common inorganic compounds that are widely used in many industrial applications such as corrosion inhibitors, reducing agents, pharmaceutical intermediates, catalysts, oxygen scavengers, emulsifiers, insecticides/herbicides, and textile dyes [1–4]. The flammable and highly explosive nature of hydrazine also made it suitable for propellants in spacecraft, rockets, and missile propulsion systems [5,6]. Despite its extensive potential applications in different sectors, long-term exposure to hydrazine in humans can cause serious health problems, especially in the lungs, brain, and central nervous system [7,8]. Not only the long-term health hazards in high concentration, but low concentration exposure can also cause dizziness, irritation of the eyes, nose, and throat, etc. [9]. As a result, the World Health Organization (WHO) categorized hydrazine as a group B2 human carcinogenic compound [10]. Therefore, it is necessary, with prime scientific significance, to develop an effective sensor system that can detect hydrazine for the protection of human health and the environment. In literature, the common methods utilized for hydrazine detection are basically colorimetry/fluorometry [11–13], chromatography [14], chemiluminescence [15], flow injection analysis [16], etc. These processes are quite time-consuming and require sophisticated instrumentation, using environmentally unfriendly solvents, sample incubation or pretreatment, etc. Thus, a nimble and viable

detection technique is much desired for the onsite monitoring of hydrazine in an easy way. In this regard, electrochemical sensing has received widespread attention owing to its easy sample preparation process, faster responses with higher sensitivity, the scope of using environment-friendly green solvents such as water-based buffer solutions, and feasible miniaturization [17–20]. Therefore, electrochemical sensing techniques have been widely utilized for the determination of hydrazine using various modified electrodes [8,9,18,21–27].

The judicious choice of electrode materials is the cornerstone for high-performance electrochemical sensing systems. Generally, the electrochemical sensing of hydrazine is based on its oxidation on the surface of the electrode. However, on the surface of the unmodified conventional bare electrode, the hydrazine oxidation is kinetically sluggish with larger oxidation overpotential and inferior current response. In this regard, developing an efficient material that can modify the conventional electrodes is worth researching as it can provide the solution to the above problems [28,29]. Accordingly, various novel nanomaterials-modified electrodes have been explored for their possible applications in electrochemical sensing [30–32].

Nanomaterials are very unique in the construction of modified electrodes as they possess very unique properties such as increased mass transport, low diffusion length, large surface-to-volume ratio, high surface reaction activity, strong adsorption ability, high electrocatalytic ability, etc. [30–36]. Thus, nanomaterials are widely used as the modified electrode compared to microelectrodes [21]. Diverse nanomaterials, including metal nanoparticles, metal oxides, or quantum dots (QDs), were developed to enable swift electron transfer in nanomaterial-modified electrode surfaces [30–36]. The QDs are very promising in this category due to their chemically tunable surface with the desired functionalities by a bottom-up approach, electron transfer efficiency, and high catalytic effect [37–41]. Owing to these abovementioned superiorities, QDs are used to detect hydrazine in some cases. Kalaivani et al. fabricated CdSe QDs@nickel hexacyanoferrate [21], Sha et al. reported biomass-derived carbon QDs [8], Qureshi et al. designed heptazine-based graphitic QDs [42], Centane et al. developed graphene QDs [43], Chen et al. studied the Au-nanoparticle containing carbon dots [44], etc. to detect/sense hydrazine electrochemically. However, the finding of new QD-based electrode materials for the electrochemical detection of hydrazine is much desired in developing an effective and high-performance detection system for neurotoxic hydrazine.

In recent years, molybdenum disulfide (MoS_2) QDs have gained tremendous attention from researchers owing to their earth abundance, high specific surface area, their higher number of edge atoms for high electrocatalytic activity, excellent photoluminescence for bioimaging superior charge trapping properties in electronics [45–48]. The more edge atoms that result in the lack of coordination of the surface atoms and unsaturated bonds are beneficial to the catalytic activity toward analytes by high surface activity and high adsorption capabilities [49,50]. To utilize these high electrocatalytic activities of MoS_2 -QDs, herein, we have synthesized the cysteine-functionalized MoS_2 -QDs by bottom-up synthesis approach to modify the Glassy Carbon Electrode (GCE) for the detection of hydrazine. The presence of cysteine functionalization can enhance the additional interaction with hydrazine for better adsorption over MoS_2 QDs-modified electrode surface and can improve the electrocatalytic oxidation of hydrazine. The electrochemical studies unveiled that this new sensor has an excellent electrocatalytic activity to oxidize hydrazine with numerous benefits such as operational simplicity, higher sensitivity, etc.

2. Materials and Methods

2.1. Chemical and Reagents

Analytical-grade reagents were purchased and used without purification for the preparation procedures. Deionized (DI) water (Millipore Milli-Q water, 18 MU cm, and 25 °C) was used wherever necessary. L-cysteine (98%), and sodium molybdate dehydrate ($\text{Na}_2\text{MoO}_4 \cdot 2\text{H}_2\text{O}$) (98%) were bought from Avra Synthesis Private Limited, India.

HCl, sodium hydroxide (NaOH), sodium dihydrogen phosphate, and disodium hydrogen phosphate were delivered by S D Fine-Chem Limited.

2.2. Synthesis of MoS₂ Quantum Dot (MoS₂ QD)

The synthesis of MoS₂ QDs was performed by adopting the reported bottom-up protocol taking the Na₂MoO₄·2H₂O and L-cysteine in a 1:2 weight ratio for complete reduction of Na₂MoO₄·2H₂O [46,47,51]. In a typical procedure, 0.25 g of Na₂MoO₄·2H₂O was first dissolved in 25 mL of water and 0.5 g of L-cysteine was dispersed in 50 mL of water, then sonicated for 10 min. Next, both solutions were mixed and sonicated for another 15 min. The pH of the mixture was then adjusted to ~6.5 by adding an HCl solution, and the dispersed L-cysteine was completely dissolved. The whitish-yellow colored solution was taken into a 100 mL Teflon-lined stainless-steel autoclave and kept at 200 °C for 36 h to complete the hydrothermal synthesis. Then the solution was cooled to room temperature and centrifuged at 14,000 rpm for 30 min. The yellow-color supernatant was collected and further filtered through 0.2 μm filter paper. The filtrate was lyophilization to provide the MoS₂ QD residue as a fluffy powder.

2.3. Characterizations

Fourier-transform infrared spectroscopy (FTIR) was carried out by making KBr pellets of the compounds using a JASCO/FTIR-4200 instrument (Tokyo, Japan). IR spectra were acquired by preparing the KBr pellet of the QD powders after sufficient drying using IR lights. The accurate size range distribution of MoS₂ QD was confirmed by High-Resolution Transmittance Microscopy (HRTEM) using the Tecnai G2, F30 (Atlanta, GA, USA) transmittance electron microscope under an accelerating potential of 300 kV.

2.4. Electrochemical Characterizations

All CV and amperometric measurements were performed using an Autolab potentiostat PGSTAT128 N (Utrecht, The Netherlands). The typical three-electrode measurement system was utilized for the measurements taking MoS₂ QD modified glassy carbon electrode as the working electrode, a Pt wire as the counter, and an Ag/AgCl as the reference electrode. The 0.1 M phosphate buffer solution (PBS) was used as the electrolyte. The MoS₂ QD-modified glassy carbon electrode was prepared by drop-casting 20 μL of MoS₂ QD solution (2 mg in 1 mL of ethanol) and subsequently dried in air and in a vacuum at 60 °C for 8 h.

3. Results and Discussion

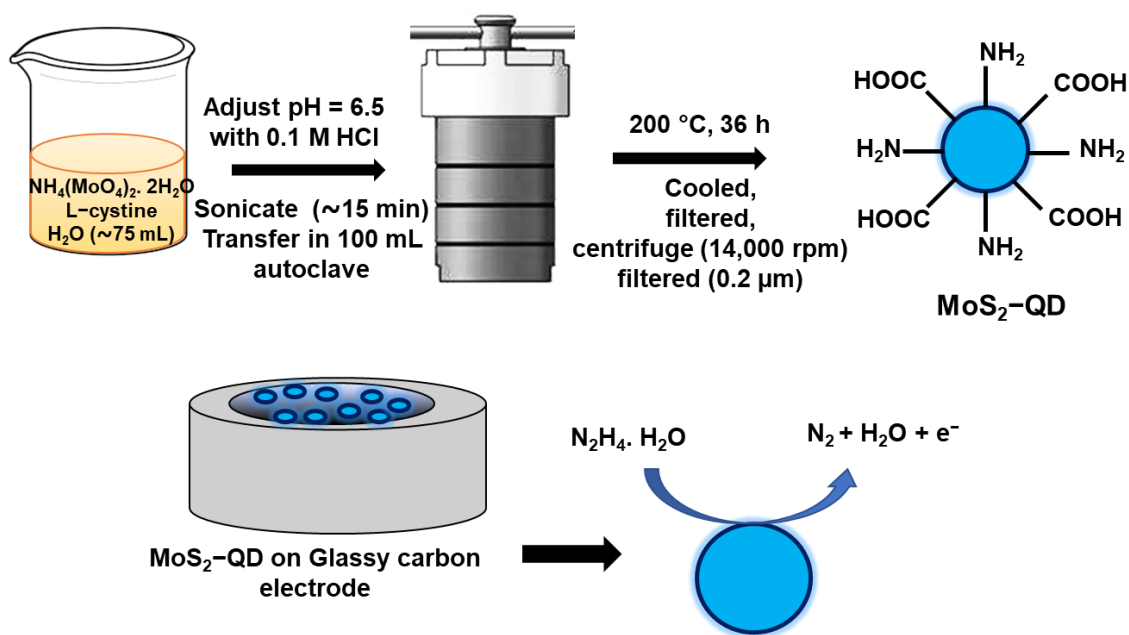
The facile bottom-up hydrothermal approach, as shown in Scheme 1, was employed to prepare the cysteine functionalized MoS₂ QDs according to our previous work [46]. The sodium molybdate precursor was reduced by the cysteine during the hydrothermal process to prepare the MoS₂ QDs. Simultaneously, the QDs are capped by cysteine, which acts as the surface passivating agent to limit agglomeration.

The HRTEM imaging study determined the morphology and size of the synthesized MoS₂ QDs. The HRTEM images are shown in Figure 1a,b. The images unveiled the homogeneously distributed spherical MoS₂ QDs. The size distribution plot of the QDs from the TEM image, as shown in Figure 1c, revealed an average particle size of 5 nm. Furthermore, HRTEM analysis in Figure 1b displayed the characteristic lattice fringes with ~0.28 nm spacing for the interplanar distance. To reach better insight, we studied the powder X-ray diffraction of the prepared MoS₂ QDs, and the plot is given in Figure 1d. The PXRD pattern revealed a highly intense peak at $2\theta = 31.8$ ($d = 0.28$ nm). Comparing with earlier literature, we concluded that the peak at $2\theta = 31.8$ is for the (101) plane [52]. The interplanar distance of the (101) plane was exactly matched with the lattice fringe of 0.28 nm evaluated from the HRTEM study. The surface capping of QDs with cysteine was further evaluated using FTIR spectroscopy by comparing the FTIR spectra of L-cysteine and MoS₂ QDs. Figure 1e unveiled the characteristic sharp peak at 1624 cm⁻¹ for the

C=O stretching of the carboxylic acid group, and a broad peak $\sim 3000\text{ cm}^{-1}$ band for O–H and N–H stretching. The presence of cysteine would provide the characteristic peaks for carboxylic acid and amino groups and the characteristic peaks of L-cysteine were retained in MoS₂ QDs. The FTIR spectra, depicted in Figure 1e, revealed a sharp peak at $\sim 1640\text{ cm}^{-1}$ owing to the C=O stretching of the carboxylic acid group from the cysteine part. Alongside this, the spectra also exhibited the other well-resolved peaks at 2195 cm^{-1} , 1570 cm^{-1} , and 1410 cm^{-1} assigned to the stretching vibrations of C–H, N–H, and C–N, respectively, present in the cysteine moieties on the surface of MoS₂. Again, the typical broad stretching vibration in the region of $\sim 3345\text{--}3440\text{ cm}^{-1}$ could be assigned to the accumulated band for O–H and N–H stretching. The presence of a small but significant peak $\sim 475\text{ cm}^{-1}$ confirmed the Mo–S vibration in MoS₂-QDs. The energy-dispersive X-ray spectroscopy (EDX) of prepared MoS₂ QDs was studied to characterize the elemental composition. The study revealed the presence of C, N, Mo, O, and S as the elements in the QDs (Figure 2). The elemental mapping also demonstrated the presence of the aforementioned materials in MoS₂-QDs.

The electrochemical characteristics of MoS₂-QDs were performed by CV measurements using a 0.1 M PBS buffer solution having neutral pH (pH ~ 7.0) as electrolyte. The bare GCE and MoS₂-QDs on GCE both revealed no oxidation peak in the absence of hydrazine, as shown in Figure 3a. However, compared to the bare GCE, MoS₂-QDs modified GCE exhibited an increment of ~ 4.5 folds higher anodic current to suggest the improved electrocatalytic efficiency of the MoS₂-QDs on GCE while using PBS solution-based electrolyte. Again, in the presence of 1 mM of hydrazine, a broad oxidation peak with little anodic current enhancement was observed in bare GCE. However, in the presence of hydrazine, the MoS₂-QDs modified GCE showed a large enhancement (~ 80 fold) in anodic current with a well-defined peak at $\sim 0.61\text{ V}$ to imply the clear oxidation of hydrazine over the MoS₂-QDs modified surface. Interestingly, in the presence of hydrazine, the voltammogram in Figure 3b revealed the absence of any reduction peak denoting the irreversible oxidation of hydrazine over MoS₂-QDs modified electrode surface. To obtain a better insight regarding the anodic current increment in the presence of hydrazine on MoS₂-QDs modified electrode surface, we studied the voltammograms of the process with stepwise addition of hydrazine starting from $100\text{ }\mu\text{M}$ to 1 mM . Figure 3b revealed the gradual increment of the anodic peak current with increasing concentration of hydrazine. The scan rate-dependent CV study of MoS₂-QDs modified GCE in the presence of 0.4 mM hydrazine revealed an increment of anodic current with increasing scan rates (Figure 3c). Again, the anodic peak current revealed a linear relation with the square root of the scan rate, as shown in Figure 3d. This linearity denoted that the electrochemical process was diffusion controlled in nature.

To evaluate the detection efficiency of the MoS₂-QDs modified electrode, the amperometric measurements of the MoS₂-QDs modified electrode were performed with the successive addition of hydrazine ($100\text{ }\mu\text{M}$ to 1 mM) at the potential of 0.61 V in 0.1 M PBS buffer electrolyte. The results are shown in Figure 4a. The anodic current at 0.61 V was gradually increased systematically upon the addition of hydrazine with a response time of $\sim 2\text{ s}$. However, we made the successive addition in 25 s intervals. The amperometric response was very stable after addition of every portion of hydrazine. The oxidation of hydrazine molecules in the presence of an aqueous 0.1 M PBS buffer to generate the nitrogen and water at the surface of the MoS₂-QDs modified electrode, as shown in Scheme 1, was the reason for the increment of the anodic current. The release of the electron in this oxidation process and the generation of oxidative species effectively increased the anodic current as the signal of the sensory system.



Scheme 1. Synthesis of MoS₂-QD and schematic of MoS₂-QD modified GCE for hydrazine electro-oxidation.

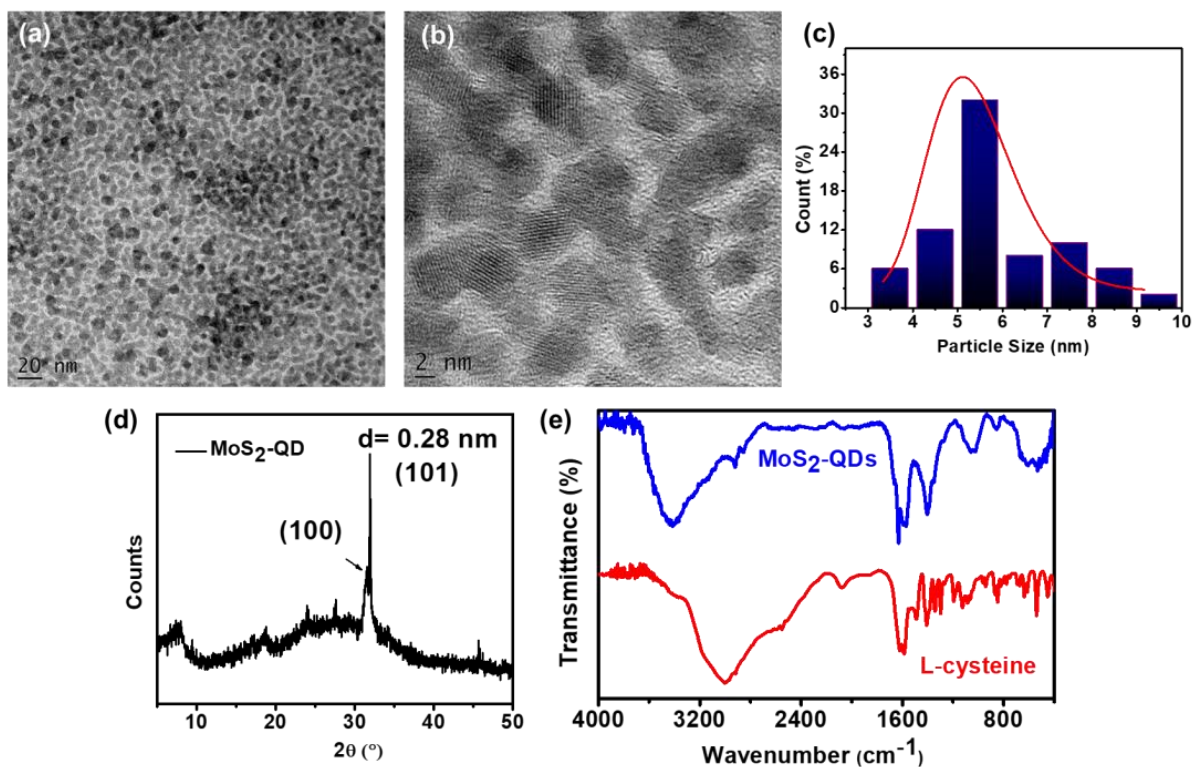


Figure 1. (a) TEM image of the MoS₂-QDs, (b) high-resolution TEM image with lattice fringes. (c) The size distribution plot of the synthesized QDs derived from the TEM image. (d) Powder XRD study of MoS₂-QDs. (e) FTIR spectra of L-cysteine and MoS₂-QDs.

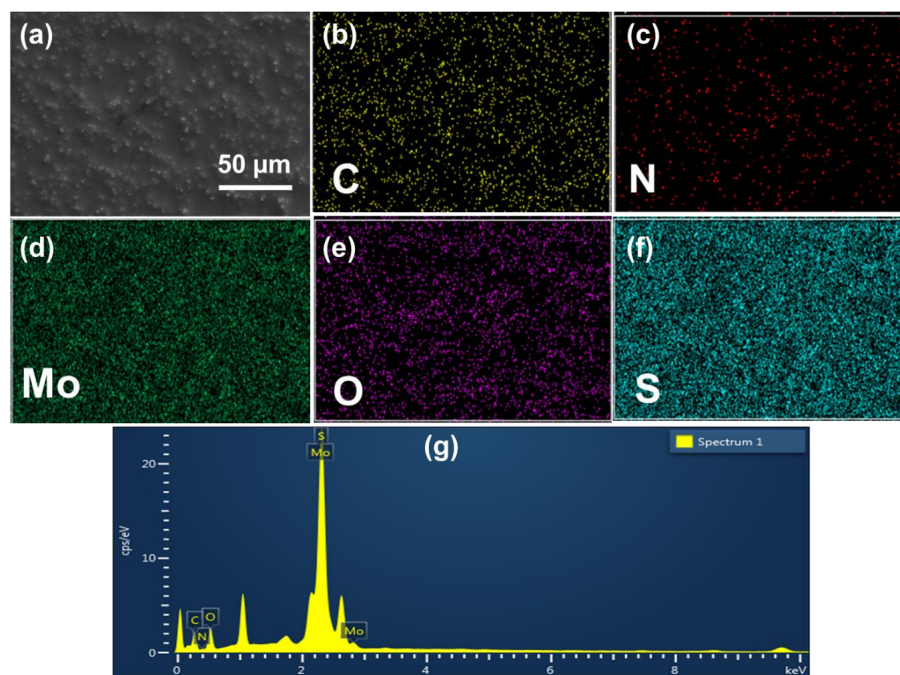


Figure 2. (a) SEM image of MoS₂ QDs and corresponding elemental mapping for (b) C, (c) N, (d) Mo, (e) O, and (f) S. (g) The EDX spectroscopy of the MoS₂-QDs.

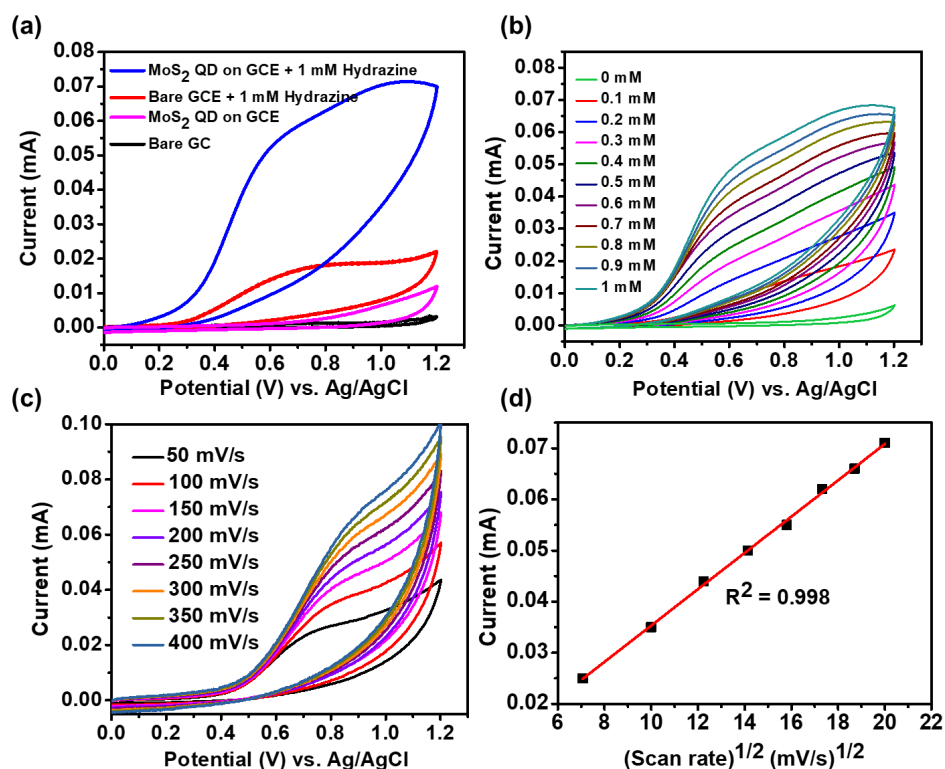


Figure 3. (a) CVs recorded of bare GCE and MoS₂-QDs modified GCE in 0.1 M PBS solution (pH 7) in the absence of hydrazine and in the presence of hydrazine at a scan rate of 100 mV/s. (b) Cyclic voltammograms of MoS₂-QDs modified GCE in the presence of different concentrations of hydrazine. Scan rate: 100 mV/s. (c) Scan rate-dependent CV study of the MoS₂-QDs modified GCE in the presence of 0.4 mM hydrazine, and (d) corresponding anodic peak current vs. square root of scan rate plot.

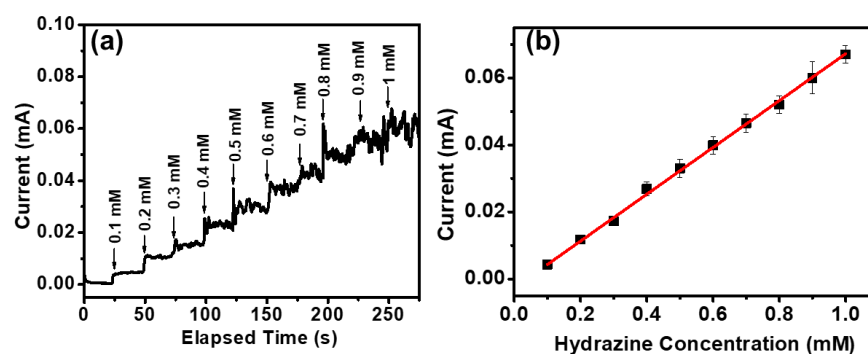


Figure 4. (a) Amperometric response of the MoS₂-QD modified GCE towards sequential addition of hydrazine at 0.61 V vs. Ag/AgCl in 0.1 M PBS solution; (b) calibration curve representing the response of MoS₂-QD modified GCE with different concentrations of hydrazine in a three-electrode system.

The calibration plot in Figure 4b revealed the linearity of current with the concentration of hydrazine. The evaluated R² value of the calibration plot was 0.998. The value confirmed the excellent linearity of the current with hydrazine concentration. The long-range of linearity (100 μM to 1 mM as measured here) of the calibration plot also denoted the better efficiency of the MoS₂-QDs modified electrode. From the slope of the calibration plot, we have derived the sensitivity and lower limit of detection (LOD) of our sensory system. The sensitivity (sensitivity = m/A where m is the slope of the plot and A is the geometrical surface area of the used electrode) was calculated as 990 μA mM⁻¹ cm⁻², which is quite higher than other reported electrochemical hydrazine sensor systems [8,18,21]. The LOD can be determined using the equation, LOD = 3 S/m, where S is the standard deviation of the response and m is the slope of the calibration plot. The calculated LOD was 34.8 μM. To highlight the sensing superiority, we have compared the sensitivity and the LODs of recently reported electrochemical hydrazine sensors in Table 1. From the table, it is envisioned that our sensory system has the potential to be used as a high-performance sensor for hydrazine, as it shows very high sensitivity and low LOD with a large linear range of detection. It should be noted that the MoS₂-QDs used here are synthesized by a single-step bottom-up hydrothermal process with a high yield. As we didn't use any precious metal nanoparticles, the MoS₂-QD-based sensing system would be economically beneficial. Again, the MoS₂-QDs-based electrode was capable of detecting hydrazine with high sensitivity, so we didn't need to add any conducting filler such as carbon nanotubes, etc. Alongside this, we employed only the simple drop-casting technique for the electrode preparation, unlike the other reports, which used sophisticated screen-printing technology, etc.

Table 1. Comparison of the performances of MoS₂-QD-based hydrazine sensors with other reported electrochemical hydrazine sensors.

Electrode Materials	Sensitivity μAmM ⁻¹ cm ⁻²	LOD	Linear Range	Reference
GO-Chitosan-Pt	104.6	3.6 μM	20 μM–10 mM	[24]
Carbon QDs	151.5	39.7 μM	125–1125 μM	[8]
Mn-hexacyanoferrate-graphite-wax	0.4753	6.65 μM	~33 μM–8 mM	[53]
MWCNT/Chlorogenic acid	4.1	-	2.5 μM–5 mM	[54]
β-nickel hydroxide nanoplatelets/CPE	1.33	0.28 μM	1–1300 μM	[5]
Pt NPs/TiO ₂ NSs/GCE	187.4	2 μM	20–900 μM	[25]
CuO/CNT/SPE	70.72	5 μM	5–50 μM	[27]
Carbon QDs	151.5	39.7 μM	125–1125 μM	[8]
Au@Pt-NFs/GO/GCE	1695.3	0.43 μM	0.8–429 μM	[23]
ferrocene-derivative/ionic liquid/CoS ₂ -CNT/CPE	0.073	0.015 μM	0.03–500 μM	[18]
N-doped Graphene-PVP/AuNPs/SPE	1.37	0.07 μM	2–500 μM	[26]
MoS ₂ -QD on GCE	990	34.8 μM	100–1000 μM	This work

4. Conclusions

In summary, a MoS₂-QD-modified GCE-based electrochemical sensing system for hydrazine detection was developed by synthesizing the MoS₂-QDs using a one-step bottom-up hydrothermal process. HRTEM images unveiled the spherical QDs with an average diameter of 5 nm. The FTIR study revealed the presence of cysteine moieties with carboxylic acid and amine groups on the surface of the QDs. The MoS₂-QD-modified GCE exhibited excellent electrocatalytic properties than bare GCE, as well as a very high sensitivity of 990 $\mu\text{A}\text{mM}^{-1}\text{cm}^{-2}$ ($R^2 = 0.998$) and low LOD of 34.8 μM towards hydrazine. The higher electrocatalytic surface area due to the smaller size of the QDs and the presence of carboxylic acid containing cysteine on the surface of the QDs enhanced the adsorption as well as the electrocatalytic activity. Finally, this high-sensitive, binder and conducting filler-free MoS₂-QD-based sensing system can be used for low-cost, nimble amperometric detection of neurotoxic hydrazine in environmental monitoring and industrial applications.

Author Contributions: Conceptualization, C.C. and S.R.; methodology, S.R., S.S., K.N.C. and C.C.; validation, S.R. and S.S.; formal analysis, investigation, S.R. and S.S.; data curation, writing, C.C.; All authors have provided critical feedback and assistance in the conducted research, analysis and finalization of the manuscript. All authors have read and agreed to the published version of the manuscript.

Funding: This research was funded by DST INSPIRE Faculty award (DST/INSPIRE/04/2016/002255).

Data Availability Statement: Data are available from the corresponding author on request.

Acknowledgments: C.C. acknowledges BITS Pilani Hyderabad Campus and DST; Govt. of India for facilities used, and S.R. acknowledges DST INSPIRE Faculty award (DST/INSPIRE/04/2016/002255) project for fellowship.

Conflicts of Interest: Authors declare no conflict of interest.

References

1. Troyan, J.E. Properties, Production, and Uses of Hydrazine. *Ind. Eng. Chem.* **1953**, *45*, 2608–2612. [[CrossRef](#)]
2. Shahid, M.M.; Rameshkumar, P.; Basirunc, W.J.; Wijayantha, U.; Chiu, W.S.; Khiew, P.S.; Huang, N.M. An electrochemical sensing platform of cobalt oxide@gold nanocubes interleaved reduced graphene oxide for the selective determination of hydrazine. *Electrochim. Acta* **2018**, *259*, 606–616. [[CrossRef](#)]
3. Rahman, M.M.; Balkhoyor, H.B.; Asiri, A.M. Ultrasensitive and selective hydrazine sensor development based on Sn/ZnO nanoparticles. *RSC Adv.* **2016**, *6*, 29342–29352. [[CrossRef](#)]
4. Zhao, S.; Wang, L.; Wang, T.; Han, Q.; Xu, S. A high-performance hydrazine electrochemical sensor based on gold nanoparticles/single-walled carbon nanohorns composite film. *Appl. Surf. Sci.* **2016**, *369*, 36–42. [[CrossRef](#)]
5. Avanes, A.; Hasanzadeh-Karamjavan, M.; Shokri-Jarcheloo, G. Electrocatalytic oxidation and amperometric determination of hydrazine using a carbon paste electrode modified with β -nickel hydroxide nanoplatelets. *Microchim. Acta* **2019**, *186*, 441–450. [[CrossRef](#)]
6. Rees, N.V.; Compton, R.G. Carbon-free energy: A review of ammonia-and hydrazine-based electrochemical fuel cells. *Energy Environ. Sci.* **2011**, *4*, 1255–1260. [[CrossRef](#)]
7. Choudhary, G.; Hansen, H. Human health perspective of environmental exposure to hydrazines: A review. *Chemosphere* **1998**, *37*, 801–843. [[CrossRef](#)]
8. Sha, R.; Jones, S.S.; Vishnu, N.; Soundiraraju, B.; Badhulika, S. A Novel Biomass Derived Carbon Quantum Dots for Highly Sensitive and Selective Detection of Hydrazine. *Electroanalysis* **2018**, *30*, 2228–2232. [[CrossRef](#)]
9. Kannan, P.K.; Moshkalev, S.A.; Rout, C.S. Electrochemical sensing of hydrazine using multilayer graphene nanobelts. *RSC Adv.* **2016**, *6*, 11329–11334. [[CrossRef](#)]
10. Rastakhiz, N.; Kariminik, A.; Soltani-Nejad, V.; Roodsaz, S. Simultaneous Determination of Phenylhydrazine, Hydrazine, and Sulfite Using a Modified Carbon Nanotube Paste Electrode. *Int. J. Electrochem. Sci.* **2010**, *5*, 1203–1212.
11. Erdemir, S.; Malkondu, S. A colorimetric and fluorometric probe for hydrazine through subsequent ring-opening and closing reactions: Its environmental applications. *Microchem. J.* **2020**, *152*, 104375–104381. [[CrossRef](#)]
12. Guria, U.N.; Manna, S.K.; Maiti, K.; Samanta, S.K.; Ghosh, A.; Datta, P.; Mandal, D.; Mahapatra, A.K. A xanthene-based novel colorimetric and fluorometric chemosensor for the detection of hydrazine and its application in the bio-imaging of live cells. *New J. Chem.* **2021**, *45*, 15869–15875. [[CrossRef](#)]

13. Liu, C.; Liu, K.; Tian, M.; Lin, W. A ratiometric fluorescent probe for hydrazine detection with large fluorescence change ratio and its application for fluorescence imaging in living cells. *Spectrochim. Acta A Mol. Biomol. Spectrosc.* **2019**, *212*, 42–47. [[CrossRef](#)] [[PubMed](#)]
14. Oh, J.-A.; Park, J.-H.; Shin, H.-S. Sensitive determination of hydrazine in water by gas chromatography–mass spectrometry after derivatization with *ortho*-phthalaldehyde. *Anal. Chim. Acta* **2013**, *769*, 79–83. [[CrossRef](#)] [[PubMed](#)]
15. Safavi, A.; Karimi, M.A. Flow injection chemiluminescence determination of hydrazine by oxidation with chlorinated isocyanurates. *Talanta* **2002**, *58*, 785–792. [[CrossRef](#)]
16. Barathi, P.; Kumar, A.S. Quercetin tethered pristine-multiwalled carbon nanotube modified glassy carbon electrode as an efficient electrochemical detector for flow injection analysis of hydrazine in cigarette tobacco samples. *Electrochim. Acta* **2014**, *135*, 1–10. [[CrossRef](#)]
17. Rana, U.; Paul, N.D.; Mondal, S.; Chakraborty, C.; Malik, S. Water soluble polyaniline coated electrode: A simple and nimble electrochemical approach for ascorbic acid detection. *Synth. Met.* **2014**, *192*, 43–49. [[CrossRef](#)]
18. Tajik, S.; Beitollahi, H.; Hosseinzadeh, R.; Afshar, A.A.; Varma, R.S.; Jang, H.W.; Shokouhimehr, M. Electrochemical Detection of Hydrazine by Carbon Paste Electrode Modified with Ferrocene Derivatives, Ionic Liquid, and CoS₂-Carbon Nanotube Nanocomposite. *ACS Omega* **2021**, *6*, 4641–4648. [[CrossRef](#)]
19. Liu, T.; Guo, Y.; Zhang, Z.; Miao, Z.; Zhang, X.; Su, Z. Fabrication of hollow CuO/PANI hybrid nanofibers for non-enzymatic electrochemical detection of H₂O₂ and glucose. *Sens. Actuators B* **2019**, *286*, 370–376. [[CrossRef](#)]
20. Dou, B.; Xu, L.; Jiang, B.; Yuan, R.; Xiang, Y. Aptamer-Functionalized and Gold Nanoparticle Array-Decorated Magnetic Graphene Nanosheets Enable Multiplexed and Sensitive Electrochemical Detection of Rare Circulating Tumor Cells in Whole Blood. *Anal. Chem.* **2019**, *91*, 10792–10799. [[CrossRef](#)]
21. Kalaivani, A.; Narayanan, S.S. Fabrication of CdSe quantum dots @ nickel hexacyanoferrate core–shell nanoparticles modified electrode for the electrocatalytic oxidation of hydrazine. *J. Mater. Sci. Mater. Electron.* **2018**, *29*, 20146–20155. [[CrossRef](#)]
22. Zhang, H.; Huang, J.; Hou, H.; You, T. Electrochemical detection of hydrazine based on electrospun palladium nanoparticle/carbon nanofibers. *Electroanalysis* **2009**, *21*, 1869–1874. [[CrossRef](#)]
23. Yang, Z.; Zheng, X.; Zheng, J. Facile synthesis of three-dimensional porous Au@Pt core-shell nanoflowers supported on graphene oxide for highly sensitive and selective detection of hydrazine. *Chem. Eng. J.* **2017**, *327*, 431–440. [[CrossRef](#)]
24. Rao, D.; Sheng, Q.; Zheng, J. Preparation of flower-like Pt nanoparticles decorated chitosan-grafted graphene oxide and its electrocatalysis of hydrazine. *Sens. Actuators B* **2016**, *236*, 192–200. [[CrossRef](#)]
25. Ding, Y.; Wang, Y.; Zhang, L.; Zhang, H.; Li, C.M.; Lei, Y. Preparation of TiO₂-Pt hybrid nanofibers and their application for sensitive hydrazine detection. *Nanoscale* **2011**, *3*, 1149–1157. [[CrossRef](#)]
26. Saengsookwaow, C.; Rangkupan, R.; Chailapakul, O.; Rodthongkum, N. Nitrogen-doped graphene-polyvinylpyrrolidone/gold nanoparticles modified electrode as a novel hydrazine sensor. *Sens. Actuators B* **2016**, *227*, 524–532. [[CrossRef](#)]
27. Rani, G.; Kumar, M. Amperometric Determination of Hydrazine Based on Copper Oxide Modified Screen Printed Electrode. *Sens. Transducers* **2018**, *223*, 22–25.
28. Baranwal, J.; Barse, B.; Gatto, G.; Broncova, G.; Kumar, A. Electrochemical Sensors and Their Applications: A Review. *Chemosensors* **2022**, *10*, 363. [[CrossRef](#)]
29. Krishnan, S. Review—Electrochemical Sensors for Large and Small Molecules in Biofluids. *J. Electrochem. Soc.* **2020**, *167*, 167505. [[CrossRef](#)]
30. Luo, X.; Morrin, A.; Killard, A.J.; Smyth, M.R. Application of Nanoparticles in Electrochemical Sensors and Biosensors. *Electroanalysis* **2006**, *18*, 319–326. [[CrossRef](#)]
31. Hanoglu, S.B.; Man, E.; Harmanci, D.; Ruzgar, S.T.; Sanli, S.; Keles, N.A.; Ayden, A.; Tuna, B.G.; Duzgun, O.; Ozkan, O.F.; et al. Magnetic Nanoparticle-Based Electrochemical Sensing Platform Using Ferrocene-Labelled Peptide Nucleic Acid for the Early Diagnosis of Colorectal Cancer. *Biosensors* **2022**, *12*, 736. [[CrossRef](#)] [[PubMed](#)]
32. Wang, J. Electrochemical biosensing based on noble metal nanoparticles. *Microchim. Acta* **2012**, *177*, 245–270. [[CrossRef](#)]
33. Priya, C.; Sivasankari, G.; Narayanan, S.S. Electrochemical behavior of Azure A/gold nanoclusters modified electrode and its application as non-enzymatic hydrogen peroxide sensor. *Colloids Surf. B Biointerfaces* **2012**, *97*, 90–96. [[CrossRef](#)]
34. Gopalan, S.A.; Anantha-Iyengar, G.; Shin-Won, K.; Shanmugasundaram, K.; Kwang-Pill, L. One Pot Synthesis of New Gold Nanoparticles Dispersed Poly(2-aminophenyl boronic acid) Composites for Fabricating an Affinity-Based Electrochemical Detection of Glucose. *Sci. Adv. Mater.* **2014**, *6*, 1356–1364.
35. Safavi, A.; Maleki, N.; Tajabadi, F.; Farjami, E. High electrocatalytic effect of palladium nanoparticle arrays electrodeposited on carbon ionic liquid electrode. *Electrochem. Commun.* **2007**, *9*, 1963–1968. [[CrossRef](#)]
36. Jeykumari, D.R.S.; Narayanan, S.S. Bionzyme Based Biosensing Platform Using Functionalized Carbon Nanotubes. *J. Nanosci. Nanotechnol.* **2008**, *9*, 5411–5416. [[CrossRef](#)]
37. Roushani, M.; Shamsipur, M.; Rajabi, H.R. Highly selective detection of dopamine in the presence of ascorbic acid and uric acid using thioglycolic acid capped CdTe quantum dots modified electrode. *J. Electroanal. Chem.* **2014**, *712*, 19–24. [[CrossRef](#)]
38. Yin, H.; Zhou, Y.; Ai, S.; Chen, Q.; Zhu, X.; Liu, X.; Zhu, L. Sensitivity and selectivity determination of BPA in real water samples using PAMAM dendrimer and CoTe quantum dots modified glassy carbon electrode. *J. Hazard. Mater.* **2010**, *174*, 236–243. [[CrossRef](#)]

39. Kalaivani, A.; Narayanan, S.S. Simultaneous Determination of Adenine and Guanine Using Cadmium Selenide Quantum Dots-Graphene Oxide Nanocomposite Modified Electrode. *J. Nanosci. Nanotechnol.* **2015**, *15*, 4697–4705. [[CrossRef](#)]
40. Zhang, C.; Wang, G.; Ji, Y.; Liu, M.; Feng, Y.; Zhang, Z.; Fang, B. Enhancement in analytical hydrazine based on gold nanoparticles deposited on ZnO-MWCNTs films. *Sens. Actuators B* **2010**, *150*, 247–253. [[CrossRef](#)]
41. Li, J.; Xie, H.; Chen, L. A sensitive hydrazine electrochemical sensor based on electrodeposition of gold nanoparticles on choline film modified glassy carbon electrode. *Sens. Actuators B* **2011**, *153*, 239–245. [[CrossRef](#)]
42. Qureshi, S.; Asif, M.; Sajid, H.; Gilani, M.A.; Ayub, K.; Mahmood, T. First-principles study for electrochemical sensing of neurotoxin hydrazine derivatives via h-g-C₃N₄ quantum dot. *Surf. Interfaces* **2022**, *30*, 101913–101922. [[CrossRef](#)]
43. Centane, S.; Sekhosana, E.K.; Matshitse, R.; Nyokong, T. Electrocatalytic activity of a push-pull phthalocyanine in the presence of reduced and amino functionalized graphene quantum dots towards the electrooxidation of hydrazine. *J. Electroanal. Chem.* **2018**, *820*, 146–160. [[CrossRef](#)]
44. Chen, W.; Wang, H.; Tang, H.; Yang, C.; Guan, X.; Li, Y. Amperometric sensing of hydrazine by using single gold nanopore electrodes filled with Prussian Blue and coated with polypyrrole and carbon dots. *Microchim. Acta* **2019**, *186*, 350–356. [[CrossRef](#)]
45. Huang, H.; Camarada, M.B.; Wang, D.; Liao, X.; Xiong, J.; Hong, Y. MoS₂ quantum dots and titanium carbide co-modified carbon nanotube heterostructure as electrode for highly sensitive detection of zearalenone. *Microchim. Acta* **2022**, *189*, 15–27. [[CrossRef](#)] [[PubMed](#)]
46. Roy, S.; Bobde, Y.; Ghosh, B.; Chakraborty, C. Targeted Bioimaging of Cancer Cells Using Free Folic Acid-Sensitive Molybdenum Disulfide Quantum Dots through Fluorescence “Turn-Off”. *ACS Appl. Bio. Mater.* **2021**, *4*, 2839–2849. [[CrossRef](#)]
47. Roy, S.; Ganeshan, S.K.; Pal, S.; Chakraborty, C. Targeted enhancement of electrochromic memory in Fe(II) based metallo-supramolecular polymer using molybdenum disulfide quantum dots. *Sol. Energy Mater. Sol. Cells* **2022**, *234*, 111487–111497. [[CrossRef](#)]
48. Li, F.; Li, J.; Cao, Z.; Lin, X.; Li, X.; Fang, Y.; An, X.; Fu, Y.; Jin, J.; Li, R. MoS₂ quantum dot decorated RGO: A designed electrocatalyst with high active site density for the hydrogen evolution reaction. *J. Mater. Chem. A* **2015**, *3*, 21772–21778. [[CrossRef](#)]
49. Kabel, J.; Sharma, S.; Acharya, A.; Zhang, D.; Yap, Y.K. Molybdenum Disulfide Quantum Dots: Properties, Synthesis, and Applications. *C* **2021**, *7*, 45. [[CrossRef](#)]
50. Yang, X.; Jia, Q.; Duan, F.; Hu, B.; Wang, M.; He, L.; Song, Y.; Zhang, Z. Multiwall carbon nanotubes loaded with MoS₂ quantum dots and MXene quantum dots: Non-Pt bifunctional catalyst for the methanol oxidation and oxygen reduction reactions in alkaline solution. *Appl. Surf. Sci.* **2019**, *464*, 78–87. [[CrossRef](#)]
51. Li, L.; Guo, Z.; Wang, S.; Li, D.; Hou, X.; Wang, F.; Yang, Y.; Yang, X. Facile synthesis of MoS₂ quantum dots as fluorescent probes for sensing of hydroquinone and bioimaging. *Anal. Methods* **2019**, *11*, 3307–3313. [[CrossRef](#)]
52. Haldar, D.; Dinda, D.; Saha, S.K. High selectivity in water-soluble MoS₂ quantum dots for sensing nitro explosives. *J. Mater. Chem. C* **2016**, *4*, 6321–6326. [[CrossRef](#)]
53. Jayasri, D.; Narayanan, S.S. Amperometric determination of hydrazine at manganese hexacyanoferrate modified graphite-wax composite electrode. *J. Hazard. Mater.* **2007**, *144*, 348–354. [[CrossRef](#)] [[PubMed](#)]
54. Salimi, A.; Miranzadeh, L.; Hallaj, R. Amperometric and voltammetric detection of hydrazine using glassy carbon electrodes modified with carbon nanotubes and catechol derivatives. *Talanta* **2008**, *75*, 147–156. [[CrossRef](#)]

Disclaimer/Publisher’s Note: The statements, opinions and data contained in all publications are solely those of the individual author(s) and contributor(s) and not of MDPI and/or the editor(s). MDPI and/or the editor(s) disclaim responsibility for any injury to people or property resulting from any ideas, methods, instructions or products referred to in the content.